ELSEVIER

Journal of Structural Geology 27 (2005) 2030–2042

JOURNAL OF STRUCTURAL GEOLOGY

www.elsevier.com/locate/jsg

Finite tectonic strain and its error, as estimated from elliptical objects with a class of initial preferred orientations

Atsushi Yamaji*

Division of Earth and Planetary Sciences, Graduate School of Science, Kyoto University, Kyoto 606-8502, Japan

Received 4 May 2004; received in revised form 9 June 2005; accepted 17 June 2005
Available online 8 August 2005

Abstract

A new inverse method is proposed to estimate strain from elliptical objects that have suffered uniform deformation with their matrix. The present method extends the applicability of strain analysis to the cases where pre-strain fabric has a class of anisotropy. Specifically, a bivariate normal distribution with the mean at the origin of the Elliott plot is expected as an approximation for the initial fabric. The method is designed to facilitate error estimation for the optimal strain ellipse. Monte Carlo tests showed that the optimal solution is accurate and numerically stable. In addition, a confidence region evaluated by the present method is also accurate, provided that the variation of initial aspect ratios was more than ~5 times larger than the deviation of the mean from the origin.

Keywords: Bivariate normal distribution; Error analysis; Fabric; Preferred orientation

1. Introduction

Ellipsoidal objects such as deformed pebbles and ooids have been used to quantify the strain of rocks including the objects with assuming uniform deformation of the rock and pre-strain random orientation of the objects (Ramsay, 1967). Extensive studies have been done for this purpose (e.g. Dunnet, 1969; Matthews et al., 1974; Borradaile 1976; Shimamoto and Ikeda, 1976; Lisle, 1977b, 1985; De Paor, 1980; Siddans, 1980). Some investigators have studied the precision of the results assuming a pre-strain random fabric (Yu and Zheng, 1984; Schultz-Ela, 1990; Hayashi, 1999; Mulchrone and Meere, 2001). Yet, real sedimentary grains have preferred orientations (Griffiths, 1967; Paterson and Yu, 1994), which can lead to significant errors in strain determination (Seymour and Boulter, 1979). The effect of pre-strain fabrics was accordingly investigated by several researchers (Elliott, 1970; Dunnet and Siddans, 1971; Ribeiro and Possolo, 1978; Wheeler, 1986).

The present article has two purposes: the presentation of a new inverse method to determine the optimal strain ellipse from deformed elliptical objects, and of the method for evaluating its error. The inverse method assumes a class of anisotropic initial fabric, and is designed deliberately to permit error estimation. The method evaluates the precision of the optimal strain ellipse. Precision is the amount of detail, and accuracy is the conformity of an estimated value to the true one (De Pree and Axelrod, 2003). The accuracy of the method is also examined using Monte Carlo tests with assumed strain ellipses. It is shown that the error estimation looses accuracy under some conditions while the optimal solution is accurate.

The present method assumes a class of pre-strain initial fabric. Namely, bivariate normal distributions on Elliott's (1970) polar plot are expected for the fabric. This assumption is supported by sedimentological studies including Potter and Pettijohn (1963), Moss (1963, 1966), Paterson and Yu (1994) and two examples described in this study.

The uniform distribution of major axis orientations have been usually assumed for the object function inversion since the pioneering work by Ramsay (1967). In this study, the pre-strain aspect ratios are shown to be as important as initial random orientations. It is demonstrated that the inversion becomes robust by including the variations of initial aspect ratios in the function. The present method allows a class of initial anisotropy.

* Tel.: +81 75 753 4150; fax: +81 75 753 4189.
E-mail address: yamaji@kueps.kyoto-u.ac.jp.

0191-8141/$ - see front matter © 2005 Elsevier Ltd. All rights reserved.
doi:10.1016/j.jsg.2005.06.007

Disregarding the initial aspect ratios has a disadvantage in evaluating the uncertainty of the strain ellipse. We assume uniform strain across a rock including the objects. If all the objects were literally spherical at the undeformed stage, their present shapes are similar to the strain ellipse (Cloos, 1947). In this case, we have no uncertainty at all. On the other hand, if the initial eccentricity is significant, initial preferred orientations become obviously important. Therefore, initial aspect ratios should not be ignored in the error estimation. For our purpose, Elliott's (1970) plot is useful.

2. Elliott plot

The shape of a grain is approximated by an ellipse with an aspect ratio, R, and the major axis orientation, ϕ, with respect to a reference line. The shape and orientation of the grain are represented by a point on the Elliott plot, the abscissa and ordinate of which are:

$$p = (\log_e R)\cos 2\phi \quad (1)$$

$$q = (\log_e R)\sin 2\phi, \quad (2)$$

respectively. The point is also represented by the position vector $\boldsymbol{x}=(p,q)$. Points on the rectangular Cartesian coordinates O–pq have one-to-one correspondence with the pairs of the shape and orientation of grains (Fig. 1). The Elliott plot is the graphical expression of the pairs. The origin, O, represents circular grains. Equant and elongate grains are plotted, respectively, near and distant from the origin. Points on the half-line, $p>0$ and $q=0$, represent grains whose major axes are parallel to the reference line ($\phi=0$). Those on the other half of the abscissa ($p<0$) represent grains whose major axes are oriented perpendicular to the line.

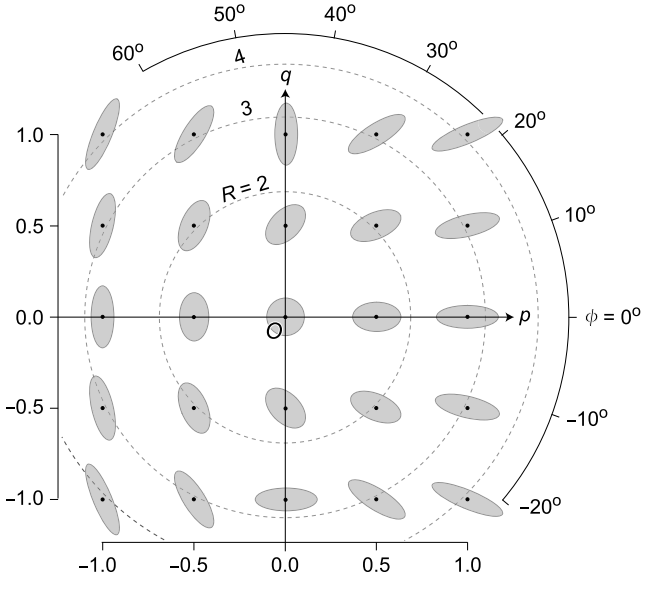

Fig. 1. Rectangular Cartesian coordinates, O–pq, to illustrate the correspondence of points on this coordinate plane with the orientation ϕ and aspect ratio R of elliptical grains. The reference orientation is parallel to the p-axis. Each gray ellipse depicts the shape and orientation corresponding to the coordinates at its center.

The Elliott plot shows not only the shape and orientation of elliptical objects but also those of the strain ellipse in question. In what follows, the pre- and post-strain parameters are distinguished by the subscripts 'i' and 'f', respectively (e.g. p_i, ϕ_i and ϕ_f). Those of strain ellipse is indicated by the subscript 's' (e.g. R_s, ϕ_s and p_s).

3. Initial fabric

Undeformed initial fabric is important for stain analysis. However, only a few sedimentologists studied (e.g. Lindsay, 1968) the relationship between the shape and orientation of sedimentary grains. It has been their convention to describe the shapes and orientations separately.

Accordingly, the present method for determining strain ellipse rests upon the observation that elongate grains are usually fewer than equant ones in undeformed clastic sediments. Moss (1963, 1966) reported that most sedimentary particles have aspect ratios between 1.3 and 2.0. Paterson and Yu (1994) described a large variation in the ratio but generally $R_i<3$ from sandstone in several depositional environments. In addition, the orientations of equant grains are insensitive to paleocurrent directions, but elongate ones have preferred orientations more often than equant ones in two-dimensional cuts (Paterson and Yu, 1994).

Accordingly, it is expected that the majority of grains will plot around the origin of the Elliott plot, and that the density of points will decrease with distance from the origin. It is, therefore, expected further that the density of points on the plot will exhibit a pattern similar to a bivariate (or two-dimensional) normal distribution.

Because of the scarce description of the relationship between the orientation and shape of sedimentary grains, I made the Elliott plots of actual examples. Fig. 2 shows the plots for sand grains in a microdelta system that was experimentally formed by Masuda and Suzaki (1984) in a large flume, 160 m long and 4 m wide. The sand used in the experiment came originally from a natural river bank in central Japan, and was composed mainly of quartz and pyroxene grains with accessories of magnetite and volcanic rock fragments. The sand was well sorted with a modal grain size at ~0.5 mm. The sand layer had foreset laminae dipping at 43°. The samples show preferred orientations, consistent with the paleocurrent direction (Masuda and Suzaki, 1984; Yamaji and Masuda, 2005).

Fig. 2a shows the plot of 1052 grains in a vertical thin section through the sediment, where horizontal paleocurrent direction is used for the reference orientation for the angle ϕ. Fig. 2b is the plot of 840 grains in a horizontal thin section, where paleocurrent direction was used for the reference orientation. In both cases, plotted points form a

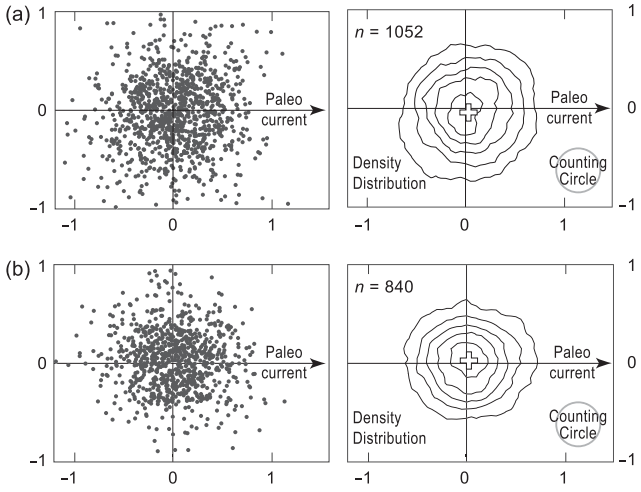

Fig. 2. The Elliott plots for grains in the vertical (a) and horizontal (b) thin sections, respectively, through an experimental microdelta system made by Masuda and Suzaki (1984). Arrows on abscissas indicate the reference orientations for the plot. Contour lines with intervals of 200 in the right panels indicate the density of plotted points counted with the moving window of the area shown by circles. Bold crosses designate the center of mass of the points.

dense cluster, and their center of mass is located in the close vicinity of the origin. The distance between the center and the origin was 0.053 and 0.034, respectively, which have the equivalent difference in aspect ratios of ~5 and ~3%.

The cluster in Fig. 2b is slightly elongated along the abscissa, indicating the abundance of grains with the major axis orientation nearly parallel and perpendicular to the paleocurrent. This accords with the description by Potter and Pettijohn (1963, p. 44) who have already pointed out that particles in the bedding plane often exhibit bimodal orientations, and the angle between the modes is ~90°.

Although these are not enough evidence, we assume that the density of points on the Elliott plot is approximated by a bivariate normal distribution with the mean at the origin. The samples were obtained from a microdelta system formed by unidirectional flow along an experimental flume, so that screening out grains with low axial ratios ($R<1.5$) enhances preferred orientations (Masuda and Suzaki, 1984). Such a preferred orientation shifts the center of mass away from the origin of the plot. Despite the strong fabrics of elongate grains, the overall pattern on the plot can be approximated by bivariate normal distributions. Grains deposited in lower energy depositional environments may satisfy the above assumption better than those in the microdelta system.

4. Bivariate normal distribution and its constant probability contours

A bivariate normal distribution has a bell-shaped probability density function, and is also characterized by ellipses, which are known as constant probability contours

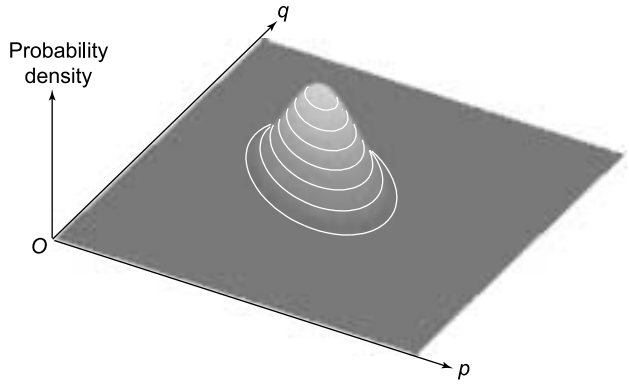

Fig. 3. Probability density of a bivariate normal distribution. White lines indicate ellipses for constant probability contours.

(Fig. 3). Let n be the number of grains, $\boldsymbol{x}^{(i)}$ the row vector for the ith point on the Elliott plot. Then

$$\bar{\boldsymbol{x}} = \frac{1}{n}[\boldsymbol{x}^{(1)} + \cdots + \boldsymbol{x}^{(n)}]$$

is the mean of the points, and the ellipse is denoted by the position vector $\boldsymbol{x}$ satisfying

$$(\boldsymbol{x}-\bar{\boldsymbol{x}})\boldsymbol{S}^{-1}(\boldsymbol{x}-\bar{\boldsymbol{x}})^{\mathrm{T}} = c^2, \tag{3}$$

where c is an arbitrary constant, $\boldsymbol{S}$ is the covariance matrix of the points and the superscript T denotes matrix transpose (Johnson and Wichern, 2002, p. 153). The ijth element of $\boldsymbol{S}$ is given by

$$S_{ij} = \frac{1}{n-1}\sum_{k=1}^{n}\left[x_i^{(k)}-\bar{x}_i\right]\left[x_j^{(k)}-\bar{x}_j\right].$$

If λ_1 and λ_2 are, respectively, the major and minor eigenvalues of $\boldsymbol{S}$, the ellipse has the radii $c\sqrt{\lambda_1}$ and $c\sqrt{\lambda_2}$. The eigenvector corresponding to λ_1 indicates the major axis orientation. The ellipse with $c^2=\chi^2(\alpha)$ contains $(1-\alpha)\times100\%$ of points, where $\chi^2(\alpha)$ is the upper (100α)th percentile of a chi-square distribution with 2 degrees of freedom. For example, the 39.35% of points fall in the ellipse with $c=1$ because $\chi^2(1-0.3935)=1$. This is the two-dimensional analogue of the 'one sigma region' of a normal distribution, of which the 68% of points fall within the range of one standard deviation from its mean.

One of the constant probability contours is defined not only by Eq. (3) but also by the five parameters a_1–a_5 (Fig. 4). Table 1 shows those parameters of the two sets of grains indicated in Fig. 2a and b. The confidence region of the mean calculated from the points is indicated by an ellipse with a specific value of c. This is used for error estimation in Section 7.

5. Transformations on the Elliott plot corresponding to strain and destrain

We assume uniform strain, meaning that all elliptical

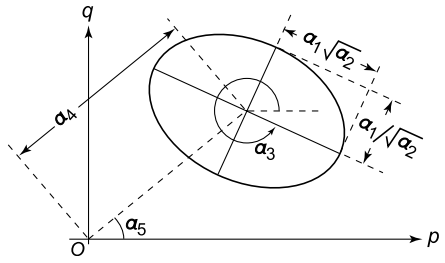

Fig. 4. Five parameters characterizing one of the ellipses in Fig. 3. The mean radius and aspect ratio are indicated by a_1 and a_2, respectively. The major-axis orientation is denoted by the angle a_3 from the horizontal axis. The parameters a_4 and a_5 indicate the position of peak of the bell-shaped surface in Fig. 3.

grains and their matrix suffered the same strain without annihilation, fission and coalescence. Mathematical equations for the deformation is obtained by combining Eqs. (1) and (2) and Ramsay's (1967, pp. 205–209) formulas

$$\tan 2\phi'_{\mathrm{f}} = \frac{2R_{\mathrm{s}}(R_{\mathrm{i}}^2-1)\sin 2\phi'_{\mathrm{i}}}{(R_{\mathrm{i}}^2+1)(R_{\mathrm{s}}^2-1)+(R_{\mathrm{i}}^2-1)(R_{\mathrm{s}}^2+1)\cos 2\phi'_{\mathrm{i}}} \tag{4}$$

and

$$R_{\mathrm{f}} = \left[\frac{\tan 2\phi'_{\mathrm{f}}(1+R_{\mathrm{i}}^2\tan^2\phi'_{\mathrm{i}})-R_{\mathrm{s}}^2(\tan^2\phi'_{\mathrm{f}}+R_{\mathrm{i}}^2)}{R_{\mathrm{s}}^2\tan^2\phi'_{\mathrm{f}}(\tan^2\phi'_{\mathrm{f}}+R_{\mathrm{i}}^2)-(1+R_{\mathrm{i}}^2\tan^2\phi'_{\mathrm{i}})}\right]^{1/2} \tag{5}$$

where $\phi'_{\mathrm{f}}=\phi_{\mathrm{f}}-\phi_{\mathrm{s}}$ and $\phi'_{\mathrm{i}}=\phi_{\mathrm{i}}-\phi_{\mathrm{s}}$. Ramsay (1967) used the ϕ_{s} orientation for the reference, but an arbitrary reference orientation is used here. Therefore, Eqs. (4) and (5) have ϕ'_{f} and ϕ'_{i} instead of ϕ_{f} and ϕ_{i}. Given a pair $(R_{\mathrm{s}},\phi_{\mathrm{s}})$ or equivalently a point $\boldsymbol{x}_{\mathrm{s}}=(p_{\mathrm{s}},q_{\mathrm{s}})$, we can calculate the final point $\boldsymbol{x}_{\mathrm{f}}=(p_{\mathrm{f}},q_{\mathrm{f}})$ from the initial one $\boldsymbol{x}_{\mathrm{i}}=(p_{\mathrm{i}},q_{\mathrm{i}})$ through the following procedure. Firstly, the pair $(R_{\mathrm{i}},\phi_{\mathrm{i}})$ is calculated via the inverses of Eqs. (1) and (2), i.e. $\phi_{\mathrm{i}}=\tan^{-1}(q_{\mathrm{i}}/p_{\mathrm{i}})$ and $R_{\mathrm{i}}=\exp[(p_{\mathrm{i}}^2+q_{\mathrm{i}}^2)^{1/2}]$. Secondly, Eqs. (4) and (5) yield the pair $(R_{\mathrm{f}},\phi_{\mathrm{f}})$, and finally, $\boldsymbol{x}_{\mathrm{f}}=(p_{\mathrm{f}},q_{\mathrm{f}})$ is obtained via Eqs. (1) and (2).

The transformation from $(p_{\mathrm{i}},\phi_{\mathrm{i}})$ to $(p_{\mathrm{f}},\phi_{\mathrm{f}})$ is a one-to-one mapping, because we assume homogeneous deformations. Therefore, the mapping $(p_{\mathrm{i}},q_{\mathrm{i}})\Rightarrow(p_{\mathrm{f}},q_{\mathrm{f}})$ is the inverse of $(p_{\mathrm{f}},q_{\mathrm{f}})\Rightarrow(p_{\mathrm{i}},q_{\mathrm{i}})$, and vice versa. In what follows, we call them the forward and backward projection of points on the Elliott plot. Equations for the backward projection are obtained by replacing R_{s} with $1/R_{\mathrm{s}}$ in Eqs. (4) and (5).

We assume that the density of points $\boldsymbol{x}_{\mathrm{i}}=(p_{\mathrm{i}},q_{\mathrm{i}})$ obeys a bivariate normal distribution with the maximum frequency at the origin for grains at undeformed state.

Therefore, it is important to see how the density distribution is transformed on the plot. Fig. 5 shows examples for a strain with axial ratio of seven applied in the orientation $\phi=0$, i.e. $R_{\mathrm{s}}=7$, $\phi_{\mathrm{s}}=0$. Such a large strain is chosen merely for highlighting the distortion of probability contours by strain.

When the density distribution of the initial points $(p_{\mathrm{i}},q_{\mathrm{i}})$ was symmetrical with respect to the origin (Fig. 5a), the post-strain distribution has oval density contours centered approximately at the point $(p_{\mathrm{s}},q_{\mathrm{s}})$, where

$$p_{\mathrm{s}} = (\log_{\mathrm{e}}R_{\mathrm{s}})\cos 2\phi_{\mathrm{s}} = \log_{\mathrm{e}}7,$$

$$q_{\mathrm{s}} = (\log_{\mathrm{e}}R_{\mathrm{s}})\sin 2\phi_{\mathrm{s}} = 0$$

Fig. 5b shows a case where the initial density distribution is elongated parallel to the X-axis of strain, which is taken parallel to the abscissa. The elliptical initial pattern indicates that many initial ellipses were oriented parallel to the principal strain axes. The resultant distribution is designated by contour lines with elongated egg-shapes. In this case, the center of mass of the points after strain

$$\bar{\boldsymbol{x}}_{\mathrm{f}} = \frac{1}{n}[\boldsymbol{x}_{\mathrm{f}}^{(1)}+\cdots+\boldsymbol{x}_{\mathrm{f}}^{(n)}] \tag{6}$$

exists at $(\log_{\mathrm{e}}(7.2),0.0)$, where n is the number of grains and $\boldsymbol{x}_{\mathrm{f}}^{(k)}$ is the kth position vector. This is, again, close to the point $(p_{\mathrm{s}},q_{\mathrm{s}})$. If the initial distribution is elongated along the ordinate (Fig. 5c), post-strain density distribution has shapes like half moon or fish scale. The initial density distribution indicates the abundance of ellipses whose major axes were rotated from the principal strain axes by 45°.

All these examples indicate that the center of mass is a first approximation for the solution $\boldsymbol{x}_{\mathrm{s}}=(p_{\mathrm{s}},q_{\mathrm{s}})$. As Lisle (1977a) pointed out, the radial component of the solution $|\boldsymbol{x}_{\mathrm{s}}|$ (namely the logarithmic strain) is closer to the harmonic mean of the aspect ratios of given ellipses than their geometric mean, and harmonic mean is always smaller than geometric mean. The latter corresponds to the radial component of $\bar{\boldsymbol{x}}_{\mathrm{f}}$, so that $|\bar{\boldsymbol{x}}_{\mathrm{f}}|$ is slightly larger than $|\boldsymbol{x}_{\mathrm{s}}|$.

Fig. 5d shows a case where elongation of the initial distribution is oblique to the strain axes. The resultant density distribution shows a pear shape, which is a rotated and warped version of the ovoid in Fig. 5b. Unlike the former cases, the resultant distribution is asymmetric with respect to the line through the origin and the center of mass. The center is deviated from $\boldsymbol{x}_{\mathrm{s}}$ not only in its radial components but also in the tangential one because of the asymmetry. Consequently, the center of mass of this case is the less accurate approximation for the strain than those of

Table 1
The parameters a_1–a_5 characterizing the ellipses with $c=1$ in Eq. (3) for the sand grains shown in Fig. 2

	a_1	a_2	a_3 (°)	a_4	a_5 (°)
Fig. 2a	0.377	1.08	48.3	0.0525	−52.9
Fig. 2b	0.329	1.13	−15.6	0.0341	49.2

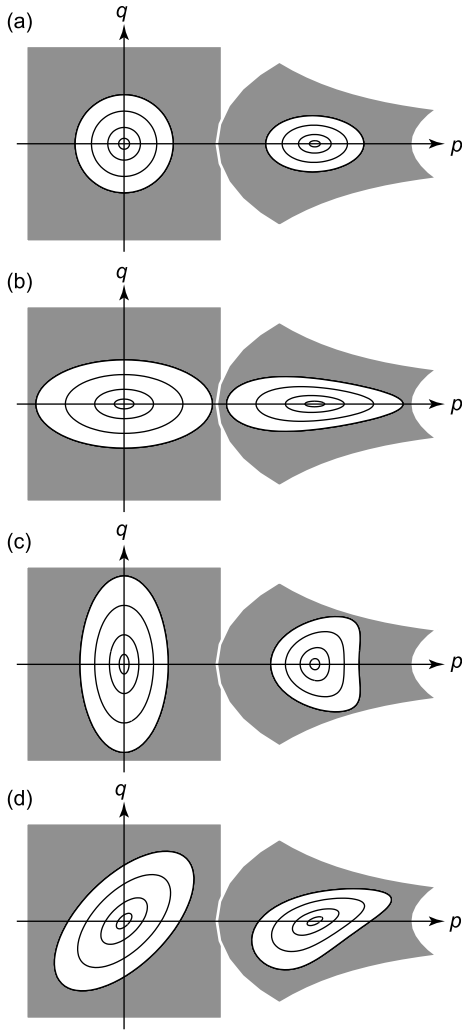

Fig. 5. Transformation on Elliott plot by pure shear with elongation parallel to the p-axis by a factor of seven. Unstrained state is shown by a circle or ellipse in a black square is centered at the origin of the plot for each panel. The square covers the region $-1 \le p \le 1$ and $-1 \le q \le 1$ on the plot. Warped cartwheel patterns in gray areas indicate the strained states. A square is transformed to a gray region by the deformation. (a) Isotropic initial fabric represented by a cartwheel pattern in a grey squares. The resultant cartwheel pattern is an oval. (b)–(d) Anisotropic initial fabrics represented by elongated patterns on Elliott plot, where density of points is indicated bivariate normal distributions.

the former cases. Such asymmetrical distributions are sometimes observed in nature reflecting pre-tectonic fabrics (Lisle, 1985, p. 17).

6. Inverse method to determine optimal strain ellipse

6.1. Theory

It is assumed that the initial density distribution of grains on the Elliott plot obeys a bivariate normal distribution with the mean at the origin. Determination of the optimal strain ellipse from deformed elliptical objects results in an inverse method under this assumption.

It has been shown in Section 5 that the initial aspect ratio and orientation of each object are calculated with Eqs. (4) and (5) from pairs of the post-strain values $R_{\mathrm{f}}^{(k)}$ and $\phi_{\mathrm{f}}^{(k)}$, $k = 1,\ldots,n$. Namely, their initial points are functions of the paired parameters of strain ellipse, R_{s} and ϕ_{s}, such that

$$p_{\mathrm{i}}^{(k)} = p_{\mathrm{i}}^{(k)}\left(R_{\mathrm{f}}^{(k)}, \phi_{\mathrm{f}}^{(k)}, R_{\mathrm{s}}, \phi_{\mathrm{s}}\right) \tag{7}$$

$$q_{\mathrm{i}}^{(k)} = q_{\mathrm{i}}^{(k)}\left(R_{\mathrm{f}}^{(k)}, \phi_{\mathrm{f}}^{(k)}, R_{\mathrm{s}}, \phi_{\mathrm{s}}\right). \tag{8}$$

The distribution of the points, which are indicated by the position vectors $\boldsymbol{x}_{\mathrm{i}}^{(k)} = \left(p_{\mathrm{i}}^{(k)}, q_{\mathrm{i}}^{(k)}\right)$, is assumed to obey a bivariate normal distribution with the mean at the origin. However, R_{s} and ϕ_{s} are chosen arbitrarily to calculate those points, so that they do not necessarily fit the expected bivariate normality. The overall misfit of the initial points $\boldsymbol{x}_{\mathrm{i}}^{(1)}, \ldots, \boldsymbol{x}_{\mathrm{i}}^{(n)}$ to a bivariate normal distribution with the mean at the origin is evaluated by Hotelling's T^2 statistic (Johnson and Wichern, 2002, p. 212),

$$T^2 = n\bar{\boldsymbol{x}}_{\mathrm{i}}\boldsymbol{S}_{\mathrm{i}}^{-1}\bar{\boldsymbol{x}}_{\mathrm{i}}^{\mathrm{T}} \tag{9}$$

where $\bar{\boldsymbol{x}}_{\mathrm{i}}$ is the mean of the initial points $\boldsymbol{x}_{\mathrm{i}}^{(1)}, \ldots, \boldsymbol{x}_{\mathrm{i}}^{(n)}$, and

$$\boldsymbol{S}_{\mathrm{i}} = \frac{1}{n-1}\sum_{k=1}^{n}[\boldsymbol{x}_{\mathrm{i}}^{(k)} - \bar{\boldsymbol{x}}_{\mathrm{i}}][\boldsymbol{x}_{\mathrm{i}}^{(k)} - \bar{\boldsymbol{x}}_{\mathrm{i}}]^{\mathrm{T}}$$

is their covariance matrix. T^2 is calculated from the initial points that depend on R_{s} and ϕ_{s} through Eqs. (7) and (8). In other words, T^2 is a function of $\boldsymbol{x}_{\mathrm{s}}$.

We expect the initial points to obey a bivariate normality. Namely, $T^2(\boldsymbol{x}_{\mathrm{s}})$ is the object function of our inverse method. The smaller the T^2 is, the better the distribution fits the bivariate normality. Therefore, the optimal parameters $\hat{R}_{\mathrm{s}}$ and $\hat{\phi}_{\mathrm{s}}$ of the strain ellipse are determined by minimizing T^2 for the n pairs of $R_{\mathrm{f}}^{(k)}$ and $\phi_{\mathrm{f}}^{(k)}$. For this optimization, we employed the downhill simplex method (Press et al., 1993). The iterative optimization started from the center of mass $\bar{\boldsymbol{x}}_{\mathrm{f}}$, because the center is a first approximation of the optimal strain (Lisle, 1977a). The inverse method was applied to artificial and natural data sets.

6.2. Artificial data

The artificial data have 100 elliptical objects. The solution that should be determined by the inversion has the values $R_{\mathrm{s}} = 5$ and $\phi_{\mathrm{s}} = 0$.

For the consideration of error estimation, distinction of the statistical terms 'sample' and 'population' is essential. For example, if 10 samples are taken from the standard normal distribution, their mean may not equal zero, which is the true mean of the distribution. The former is the sample mean, and the latter is the population mean. The former approaches the latter by increasing number of samples. Likewise, sample covariance and population covariance should be distinguished.

The artificial dataset was generated as follows. First, the points $\boldsymbol{x}_{\mathrm{i}}^{(1)},\ldots,\boldsymbol{x}_{\mathrm{i}}^{(100)}$ representing the initial fabric were distributed on the *O–pq* plane with the zero population mean and a population covariance. The dispersion of the points shows anisotropy (Fig. 6a), because the covariance matrix of the points had deviatoric components with significant magnitudes. Second, the forward projection of the points with the prescribed parameters $R_{\mathrm{s}}=5$ and $\phi_{\mathrm{s}}=0$ yielded the points $\boldsymbol{x}_{\mathrm{f}}^{(1)},\ldots,\boldsymbol{x}_{\mathrm{f}}^{(100)}$ (Fig. 6b). The inverse method was applied to the ellipses that were denoted by those post-strain points.

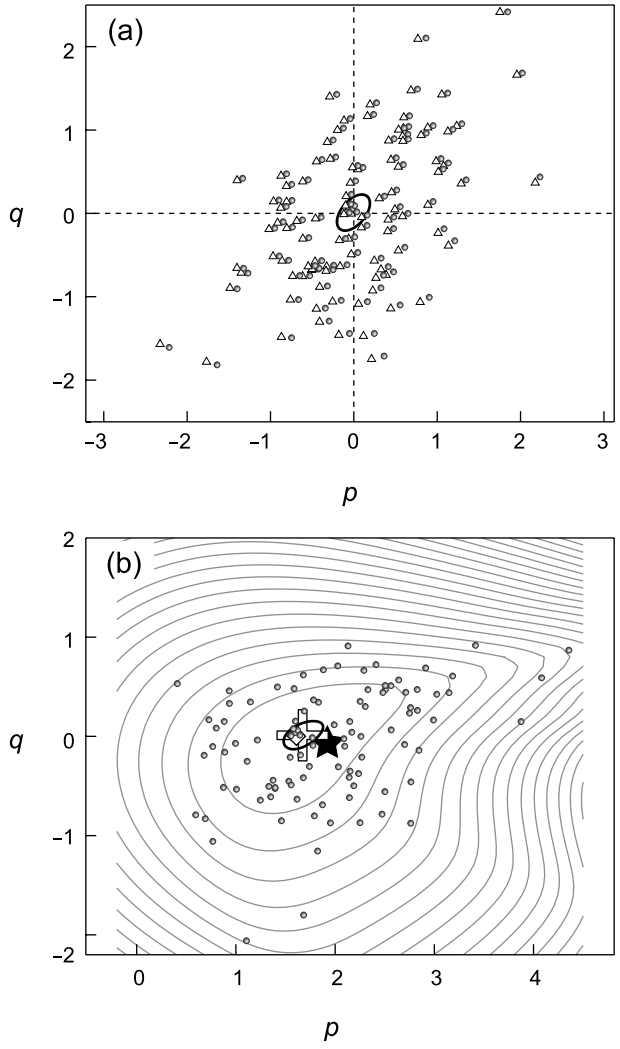

Fig. 6. (a) The Elliott plots of the points $\boldsymbol{x}_i^{(1)},\ldots,\mathrm{x}_i^{(100)}$ representing pre-strain ellipses of an artificial example. Small open circles designate the ellipses. Thick line encircling the origin illustrates the 95% confidence region of the mean $\bar{\boldsymbol{x}}_i$ inferred from the points. Triangles indicate the points that were projected backward from the post-strain ellipses with the optimal strain parameters. (b) The Elliott plot of the post-strain ellipses for the artificial data. Diamond and cross indicate the assumed and optimal strains, the latter of which was determined from the post-strain ellipses using the present method. Gray lines indicate the contours of T^2 statistic. Thick line encircling the optimal point shows the 95% confidence region of the optimal strain. The optimal strain determined by the θ-curve method (Lisle, 1977b) is denoted by a star.

Fig. 6b shows the result. The surface defined by the object function $T^2(p_{\mathrm{s}},q_{\mathrm{s}})$ is indicated by contours. The optimal strain ellipse coincides with the minimum point of the surface. The optimal strain ellipse has the values $\hat{R}_{\mathrm{s}}=5.3$ and $\hat{\phi}_{\mathrm{s}}=0.3°$, which approximate the assumed values $R_{\mathrm{s}}=5$ and $\phi_{\mathrm{s}}=0$. Namely, the inverse method was successful.

The small errors in these parameters came from the disagreement between the population mean and sample mean of $\boldsymbol{x}_{\mathrm{i}}^{(1)},\ldots,\boldsymbol{x}_{\mathrm{i}}^{(100)}$. The inversion assumed that their mean is located at the origin, but the actual sample mean was displaced from the origin by 0.080 on the Elliott plot. Solid triangles in Fig. 6a indicate the points that were projected backward from points $\boldsymbol{x}_{\mathrm{f}}^{(1)},\ldots,\boldsymbol{x}_{\mathrm{f}}^{(100)}$ with the optimal strain. If the inverse method had determined the correct values, the triangles would have occupied the same positions with the open circles. The disagreement of the population and sample means was the origin of the error of the inverse method. The Euclidean distance of the optimal point $\hat{\boldsymbol{x}_{\mathrm{s}}}=(\hat{p_{\mathrm{s}}},\hat{q_{\mathrm{s}}})$ from the assumed one $\boldsymbol{x}_{\mathrm{s}}=(p_{\mathrm{s}},q_{\mathrm{s}})$,

$$d=|\hat{\boldsymbol{x}_{\mathrm{s}}}-\boldsymbol{x}_{\mathrm{s}}| \tag{10}$$

is a measure of the error, and is 0.067 for this example.

6.3. Natural data

The natural dataset came from the deformed ooids whose photomicrograph is shown in the textbook by Ramsay and Huber (1983, p. 83). The natural data were chosen, here, to show that the present inverse method works well if the bivariate normality is an approximation for pre-strain fabric.

The optimal strain determined by the present method had the parameters $\hat{R}_{\mathrm{s}}=1.51$ and $\hat{\phi}_{\mathrm{s}}=-46.9°$, which are approximately equal but different from the solution given by Ramsay and Huber (1983) using their graphical R_{f}/ϕ method (Fig. 7). Their solution had the parameters, $R_{\mathrm{s}}=1.7$ and $\phi_{\mathrm{s}}=-42°$. The difference probably resulted from my measurement of R_{f} and ϕ_{f} for each grain on the photomicrograph. This is demonstrated by the optimal solution determined from the same dataset through the θ-curve method (Lisle, 1977b). This solution had the parameters $\hat{R}_{\mathrm{s}}=1.55$ and $\hat{\phi}_{\mathrm{s}}=-47.8°$, and the corresponding point $\hat{\boldsymbol{x}_{\mathrm{s}}}$ fell within the 95% confidence region of the solution of the present method. The method for determining the region is explained in Section 7.

The approximate coincidence of the optimal solutions yielded by those three methods shows that all the methods worked for this dataset. The data were suitable for the θ-curve and graphical R_{f}/ϕ methods. Namely, the points, $\boldsymbol{x}_{\mathrm{f}}^{(k)}$ ($k=1,\ldots,n$), make a cluster that is elongated approximately parallel to the ray from the origin through the cluster center. The elongation is depicted by the ellipse that is shown by a dotted line in Fig. 7a. In addition, the cluster of inferred pre-strain points is elongated along the strain axis ϕ_{s}. In other

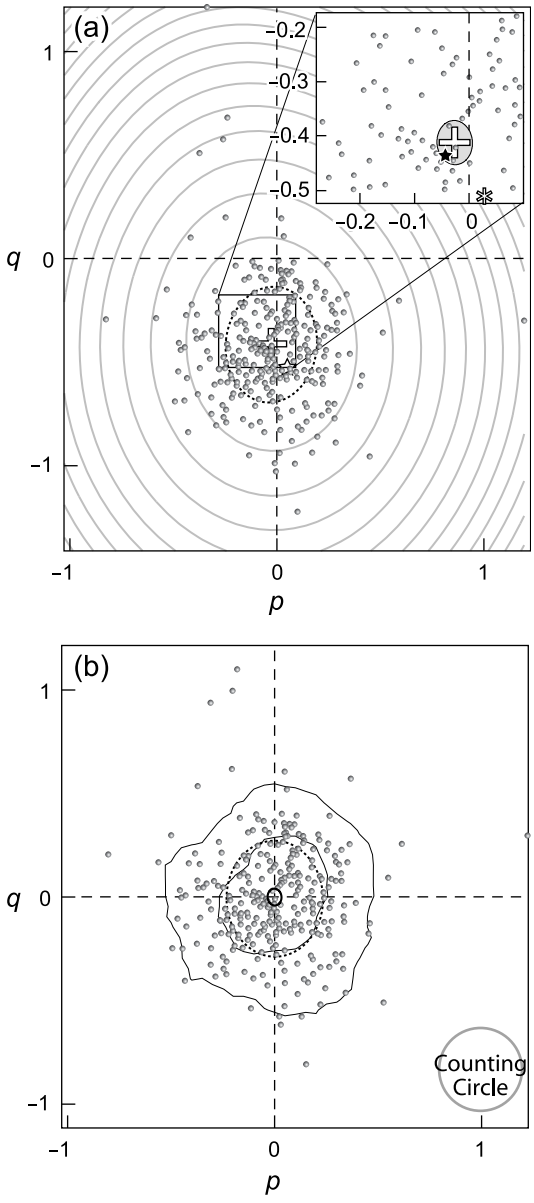

Fig. 7. (a) The Elliott plot of the R_f/ϕ data measured from a photomicrograph of deformed ooids in Ramsay and Huber (1983). Dotted line designates the ellipse $(\bar{\boldsymbol{x}}_f-\boldsymbol{x})\boldsymbol{S}_f^{-1}(\bar{\mathrm{x}}_f-\boldsymbol{x})^T=1$. Gray lines indicate the contours of T^2 statistic, and bold cross at the minimum point of T^2 indicates the optimal strain. Inset shows the 95% confidence region of the optimal strain. The solution presented by Ramsay and Huber (1983) is depicted by an asterisk. The optimal strain determined by the θ-curve method is indicated by a star. (b) The initial points $\hat{\boldsymbol{x}}_i^{(1)},\ldots,\hat{\boldsymbol{x}}_i^{(n)}$ obtained from the data in (a) with the optimal strain. Thick line surrounding the origin depicts the 95% confidence region of the mean for the points. Dotted line around the origin indicates the ellipse defined by $\boldsymbol{x}\boldsymbol{S}_i^{-1}\boldsymbol{x}^T=1$. Thin lines encompassing the origin are the contours showing the number density of points at 10 and 50 that were evaluated with the counting circle.

words, the initial fabric had weak anisotropy, but the parallelism was favorable to the two methods.

Obviously, the bivariate normality is a first approximation for the initial points (Fig. 7b). The two contour lines designated in the subfigure are only approximately similar to the ellipse $\boldsymbol{x}_i\boldsymbol{S}_i^{-1}\boldsymbol{x}_i^T=1$. Accordingly, the present method satisfactorily worked. The method does not require strict bivariate normality but a single cluster with the maximum density around the cluster center.

7. Error analysis

There are three origins of error in the results of the present method. First, heterogeneous deformation violates our basic assumption. Second, the bivariate normality may not be a good approximation for initial fabric. The mixture of, e.g. pieces of porous pumice and denser silici-clastic grains that behave differently in water current may not exhibit the bivariate normality. Third, even if the normality holds, the population or sample mean may not coincide with the origin of the Elliot plot. These factors give rise to inaccuracy of our optimal solution. The true strain is not observable, so that the accuracy cannot be determined. We proceed to estimate the precision rather than accuracy by assuming the bivariate normality and a homogeneous deformation.

7.1. Theory

The optimization was done with the assumption that $\boldsymbol{x}_i^{(1)},\ldots,\boldsymbol{x}_i^{(n)}$ were occurrences from a bivariate normal distribution with the population mean at the origin. Let $\hat{\boldsymbol{x}_i}^{(k)}$ be the initial point of the kth elliptical object that is inferred with the optimal strain $\hat{\boldsymbol{x}_s}$, then $\hat{\boldsymbol{x}_i}=\sum_k^n\hat{\boldsymbol{x}_i}^{(k)}/n$ is the mean of the initial points. Our inversion adjusts the mean to the origin, but it should be noted that we do not obtain the population mean but the sample mean $\bar{\boldsymbol{x}}_i$ of the points $\hat{\boldsymbol{x}}_i^{(1)},\ldots,\hat{\boldsymbol{x}}_i^{(n)}$. The population mean can be estimated from the sample mean with uncertainty, which is in turn propagated to the uncertainty of the optimal strain. Therefore, we estimate the uncertainty of the optimal strain from that of the population mean.

The uncertainty of the population mean is depicted by the confidence region of the population mean. If the mean exists at a probability of $1-\alpha$ in a region, the region is said to be a $100(1-\alpha)\%$ confidence region. If the points $\hat{\boldsymbol{x}}_i^{(1)},\ldots,\hat{\boldsymbol{x}}_i^{(n)}$ obey bivariate normality, this confidence region is indicated by the ellipse around $\bar{\boldsymbol{x}}_i$ that is defined by all $\boldsymbol{x}$ such that

$$n(\bar{\boldsymbol{x}}_i-\boldsymbol{x})\hat{\boldsymbol{S}}_i^{-1}(\bar{\boldsymbol{x}}_i-\boldsymbol{x})^T\le 2\left(\frac{n-1}{n-2}\right)F_{2,n-2}(\alpha) \tag{11}$$

where $\hat{\boldsymbol{S}}_i$ is the sample covariance determined from $\hat{\boldsymbol{x}}_i^{(1)},\ldots,\hat{\boldsymbol{x}}_i^{(n)}$, and $F_{2,n-2}(\alpha)$ is the inverse of the F cumulative distribution function with 2 and $n-2$ degrees of freedom (Johnson and Wichern, 2002, p. 221). For example, substituting $\alpha=1-0.3935=0.6065$ into this equation, we obtain a standard (39.35%) confidence region centered at the point $\bar{\boldsymbol{x}}_i$. Given a bivariate normal distribution, the 39.35% confidence region corresponds to the area of 'one

standard deviation' (Kanatani, 1996, p. 123). If $\lambda^{(i)}$ and $\boldsymbol{e}^{(i)}$ are the ith eigenvalue and eigenvector pair of $\hat{\boldsymbol{S}}_{\rm i}$, the major and minor radii of the confidence ellipse are given by

$$\left[\lambda^{(i)}\frac{2(n-1)}{n(n-2)}F_{2,n-2}(\alpha)\right]^{1/2}\boldsymbol{e}^{(i)} \tag{12}$$

where $i=1$, 2 and $|\boldsymbol{e}^{(i)}|=1$.

The closed loop that is defined by the forward projection of this confidence ellipse can be used as the confidence region of the optimal point $\hat{\boldsymbol{x}}_{\rm s}$. The following Monte Carlo tests demonstrate that this is a good approximation for the $100(1-\alpha)\%$ confidence region provided that the true $\bar{\boldsymbol{x}}_{\rm i}$ is close to the origin.

The resultant confidence region around the optimal point has one of the shapes in Fig. 5, namely, they are an ovoid, semilunar, crescent, or screwed ovoid. Let $\hat{\varepsilon}$ and $\hat{\psi}$ be the radial and tangential components of the optimal point $\hat{\boldsymbol{x}}_{\rm s}$. The former component indicates logarithmic strain. The upper and lower error bounds for the aspect ratio and major axis orientation of the optimal strain ellipse are defined as follows. First, the circles that inscribe and circumscribe the confidence region are drawn to determine $\Delta_1\varepsilon$ and $\Delta_2\varepsilon$ (Fig. 8). The sector that has the apex at the origin with the smallest apical angle to include the region is also used to define $\Delta_1\psi_{\rm s}$ and $\Delta_2\psi_{\rm s}$. The former pair are transformed into the lower and upper confidence limits for the optimal aspect ratio as $\hat{R}_{\rm s}/\exp(\Delta_1\varepsilon)$ and $\hat{R}_{\rm s}/\exp(\Delta_2\varepsilon)$. Those of the optimal major axis orientation $\hat{\phi}_{\rm s}$ are $(\hat{\psi}_{\rm s}-\Delta_1\psi_{\rm s})/2$ and $(\hat{\psi}_{\rm s}+\Delta_2\psi_{\rm s})/2$. If the confidence region includes the origin, these error bounds become indeterminate.

7.2. Examples

7.2.1. Artificial data

The 95% confidence region of the mean was determined by Eq. (12) for the artificial data introduced in Section 6.2. The small ellipse centered at the origin in Fig. 6a shows the region. The region was transformed forward with the optimal strain. The oval of which center is indicated by a cross in Fig. 6b shows the 95% confidence region of the optimal strain $\hat{\boldsymbol{x}}_{\rm s}$. The diamond in the subfigure depicts the assumed strain, which is successfully included in the confidence region. The optimal solution and its 95% confidence intervals are $\hat{R}_{\rm s}=5.3^{+0.7}_{-0.6}$ and $\hat{\phi}_{\rm s}=0.26^{\circ+5.7^{\circ}}_{-4.5^{\circ}}$. True values $R_{\rm s}=5$ and $\phi_{\rm s}=0^{\circ}$ are included in these intervals.

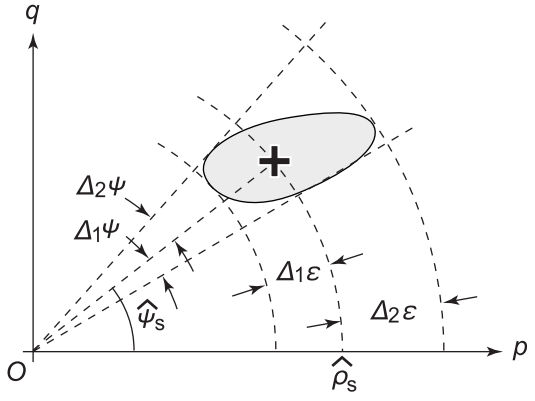

Fig. 8. Error bounds for the radial and tangential components of the Elliott plot defined by a confidence region (gray) of the optimal point (cross).

7.2.2. Natural data

The oval centered by a cross in the inlet of Fig. 7a shows the 95% confidence region of the optimal strain. The region was obtained by the forward projection of the 95% confidence region of $\bar{\boldsymbol{x}}_{\rm i}$, which is shown by the small ellipse around the origin in Fig. 7b. The optimal strain has the confidence intervals, $\hat{R}_{\rm s}=1.51\pm0.06$ and $\hat{\phi}_{\rm s}=-46.9^{\circ+9.1}_{-9.2}$, which include the optimal strain determined by the θ-curve method.

Ignoring the few widely scattered points, Ramsay and Huber (1983, p. 82) used the extent of the cluster on their $R_{\rm f}/\phi$ diagram as the 'fluctuation' of the major-axis orientation of the optimal strain. They presented a value of about 60° for the fluctuation. The angle that is subtended by the ellipse $(\bar{\boldsymbol{x}}_{\rm f}-\boldsymbol{x})\boldsymbol{S}_{\rm f}^{-1}(\bar{\boldsymbol{x}}_{\rm f}-\boldsymbol{x})^{\rm T}=1$ from the origin in Fig. 7a is about 69°, comparable with the fluctuation. Note that the size of cluster is insensitive to the number of data, n, but the precision of the optimal strain is improved by increasing n. Ramsay and Huber(1983) neglected this statistical effect. In contrast, the confidence region given by Eq. (12) diminishes in size with increasing n.

8. Monte Carlo tests

In order to verify the confidence region of the optimal point, two series of Monte Carlo tests were conducted. Points $\boldsymbol{x}_{\rm i}^{(1)},\ldots,\boldsymbol{x}_{\rm i}^{(n)}$ were firstly distributed on the Elliott plot with prescribed population parameters of a_1–a_5 that characterize the ellipse defined by Eq. (3) where $c=1$, and secondly the ellipses represented by the points were strained, and finally the optimal strain ellipse was compared with the assumed one. The parameter $\phi_{\rm s}$ was fixed at zero, while $n=20$–100 and $R_{\rm s}=1$–20 were treated as random variables. The parameters a_1–a_5 were also treated as random variables. Values for a_1 were assigned from a uniform random sequence between 0 and 1.5. This upper bound was chosen to have enough capacity for the area of one standard deviation, because most sedimentary grains have $\log_{\rm e}R_{\rm i}$ between 0.26 and 0.69 (Moss, 1963, 1966).

The first series of the Monte Carlo tests was conducted with the population mean fixed at the origin, namely, $a_4=0$. In the second series, the mean was treated as random variable obeying another bivariate normal distribution with the population covariance

$$\begin{pmatrix}0.07^2 & 0.00\\ 0.00 & 0.07^2\end{pmatrix}$$

and with the population mean at the origin. Goodness of the optimal solution to the correct solution was estimated by the distance d.

8.1. Series 1

The population mean of the initial points of the first series was fixed at the origin. The validity of our error estimation was tested by the following two quantities, $\bar{d}$ and m_{39}. The former, $\bar{d}$, is defined as the average of ds for 50 data sets with the same combination of the variables, n, R_s, a_1, a_2 and a_3, where d was calculated using Eq. (10) for each data set. This average was evaluated with 1000 combinations of the variables. It was demonstrated consequently that $\bar{d}$ is primarily determined by n and a_1 (Table 2). It is natural that increasing n decreases the representative misfit $\bar{d}$ as the negative correlation coefficient indicates (Fig. 9). Interestingly, $\bar{d}$ shows convergence to zero as $a_1 \to 0$. Namely, the precision of strain ellipse is improved by decreasing variation of R_i.

For each of the 50 data sets, the optimal point and its standard confidence region were calculated to see if the region included the assumed point $\boldsymbol{x}_s$. The quantity m_{39} is defined as the ratio of the counts of this inclusion in the 50 trials. For the ideal case, m_{39} should be equal to 0.39, because we use the standard confidence region of the optimal strain $\hat{\boldsymbol{x}_s}$. The value of 39% was chosen instead of 95%, because the latter is close to the upper limit, i.e. 100%.

It was found that m_{39} has little correlation (correlation coefficient <0.1) with the random variables except for a_1. Fig. 9c shows m_{39} versus a_1, indicating a linear correlation with the correlation coefficient of 0.79 and the intercept at $m_{39}=0.36$, which is very close to 39%. Therefore, if the variation of R_i is small, the present method yields a satisfactory estimate of the standard confidence region. The parameter m_{39} has a tendency to increase with a_1, meaning that our confidence region is somewhat larger than the true standard confidence region of the optimal point.

These observations demonstrate that our error estimation works well to determine the optimal strain ellipse, if the population mean was placed at the origin. The confidence region is somewhat overestimated in size.

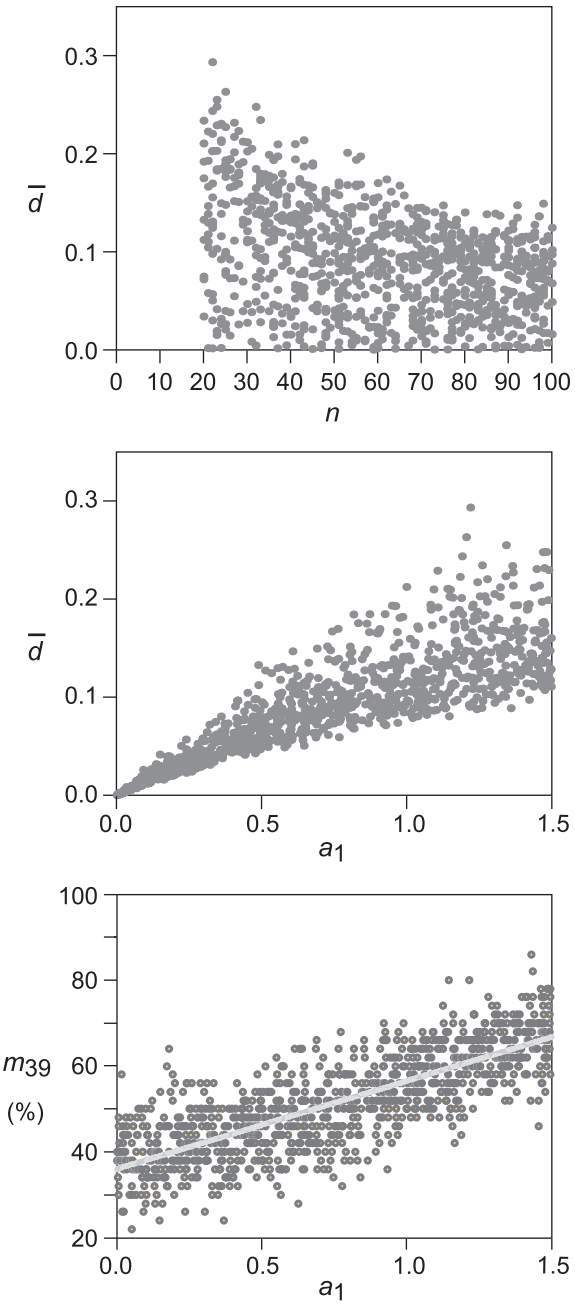

Fig. 9. Scatter plots showing the relationship among n, a_1, $\bar{d}$ and m_{39} for the first series of Monte Carlo tests. The parameter a_1 represents the variation of aspect ratios at pre-strain stage, and $a_1=0$ indicates that all grains were circular. The regression line is indicated by a light gray line in the third panel and by the equation $m_{39}=0.21a_1+0.36$.

8.2. Series 2

The second series of the Monte Carlo tests were conducted with $a_4 \geq 0$: the population mean was not fixed

Table 2
Correlation coefficients for the first and second series of Monte Carlo tests

		n	R_s	a_1	a_2	a_3	a_4	a_5
Series 1	$\bar{d}$	−0.40	0.02	0.85	0.07	−0.02		
	m_{39}	0.02	0.02	0.79	−0.03	−0.03		
Series 2	$\bar{d}$	−0.36	0.00	0.45	−0.06	0.03	−0.66	−0.01
	m_{39}	−0.15	0.00	0.83	−0.02	0.01	−0.37	−0.01

at the origin. The displacement of the population mean violates the assumption of our inverse method, and might spoil the optimal solution. Accordingly, the aim of this series of tests was to see the robustness of the method. The sample values for a_4 had a range from 0.0 to 0.35 with the mode at ~0.1. This range is one order of magnitude greater than the accrual a_4 for the sedimentary grains shown in Fig. 2 and Table 1.

It was seen that the parameters d and $\bar{d}$ had correlation coefficients greater than 0.1 only with n, a_1 and a_4 (Table 2). Fig. 10 shows the relationship of $\bar{d}$ and m_{39} with the parameters a_1 and a_4. The average accuracy $\bar{d}$ had lower bounds slightly smaller than a_4 (Fig. 10b). For the full ranges of a_1 and a_4, $\bar{d}$ was smaller than ~0.3, which corresponds to a ~35% difference in R_s (because $e^{0.3} = 1.35$) or an angular difference of (arcsin 0.3)/2 ≈ 8.7° for ϕ_s.

In contrast, the increase of a_4 causes a drastic change in m_{39} (Fig. 10c and d). While a_1/a_4 is greater than ~6, m_{39} exhibited a good correlation with a_1. In this case, our error estimation gives a good approximation for the standard confidence region of the optimal solution. However, m_{39} fell significantly from the expected value for $a_1/a_4 \lesssim 4$, and m_{39} approached zero with decreasing a_1/a_4. The transition occurred at the ratio $a_1/a_4 \approx 5$.

The second series of the Monte Carlo tests demonstrates that the optimal point has an average error $\bar{d}$ slightly smaller than a_4. However, the error estimation becomes unstable for $a_1/a_4 \lesssim 5$, while $\bar{d}$ remains small, i.e. the inverse method is robust for the variations of a_4 despite the basic assumption ($a_4 = 0$) of the method, but the error estimation becomes difficult for larger a_4. The grains shown in Fig. 2a and b have the ratio a_1/a_4 at 7.2 and 9.6, therefore, the error estimation would be successful if those grains are strained.

9. Comparison with R_f/ϕ technique

The θ-curve method (Lisle, 1977b), a computerized version of the R_f/ϕ technique, is often employed to evaluate strain ellipses. However, this method has computational instability in determining the optimal strain, while the optimal strain determined by the present method is stable.

The θ-curve method assumes a uniform distribution for ϕ_i, and minimizes the object function

$$\chi^2(\boldsymbol{x}_s) = \sum_{i=1}^{m} \frac{[N_i(\boldsymbol{x}_s) - n/m]^2}{n/m} \tag{13}$$

for obtaining the optimal $\boldsymbol{x}_s$, where N_i is the number of elliptical objects whose initial orientations were in the ith bin, and m is the number of bins with the configurations suggested by Lisle (1985, p. 19). N_i is a function of $\boldsymbol{x}_s$. $\chi^2(\boldsymbol{x}_s)$

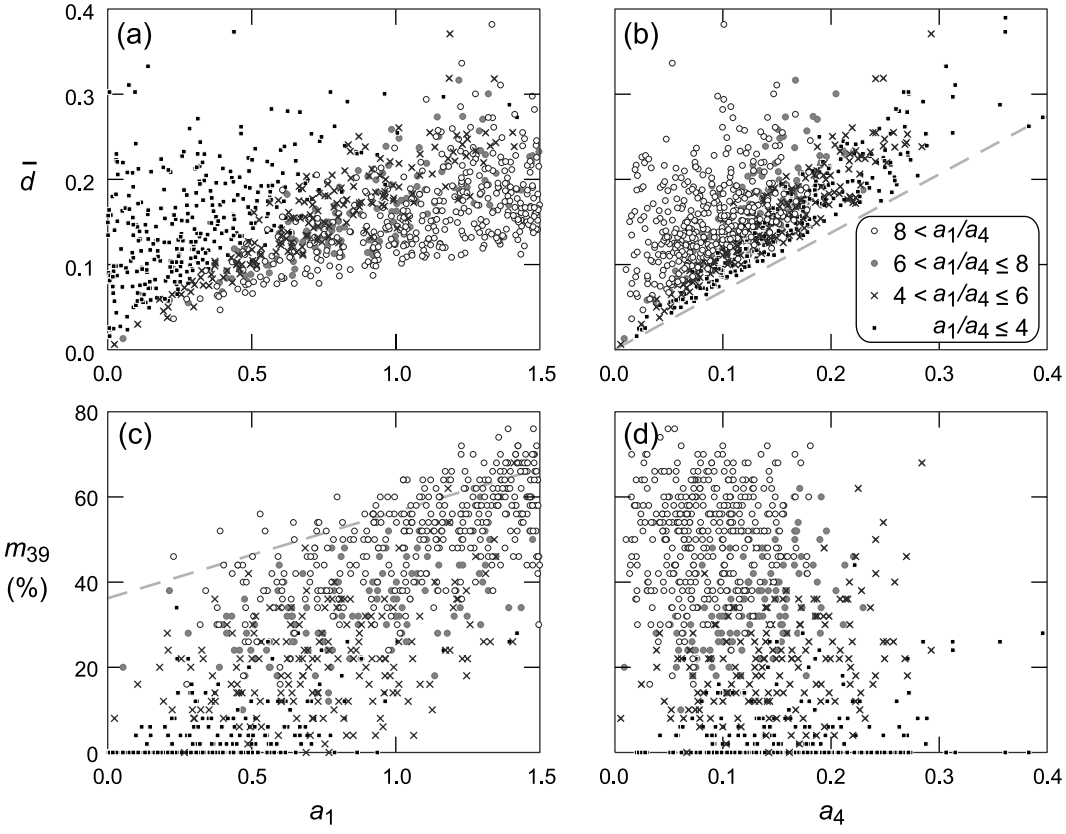

Fig. 10. Scatter plots showing the relationship between a_1, a_4, $\bar{d}$ and m_{39} for the second series of Monte Carlo tests. Dashed line in (b) delineates the lower limit of $\bar{d}$, and that in (c) shows the regression line in Fig. 9. Note the deviation of points from the regression line by the decreasing ratio of a_1/a_4.

is the chi-square statistic to evaluate how the initial orientations were uniform (Lisle, 1977b).

The method was applied to the artificial data $\boldsymbol{x}_{\mathrm{f}}^{(1)}, \ldots, \boldsymbol{x}_{\mathrm{f}}^{(100)}$ that were generated from an isotropic initial fabric. Fig. 11a shows the optimal point and the contours of $\chi^2(\boldsymbol{x}_{\mathrm{s}})$. Owing to the uniform initial fabric, the method was successful in yielding the optimal point close to the assumed one (Fig. 11b), though the optimal point obtained by the present method was closer to the assumed one.

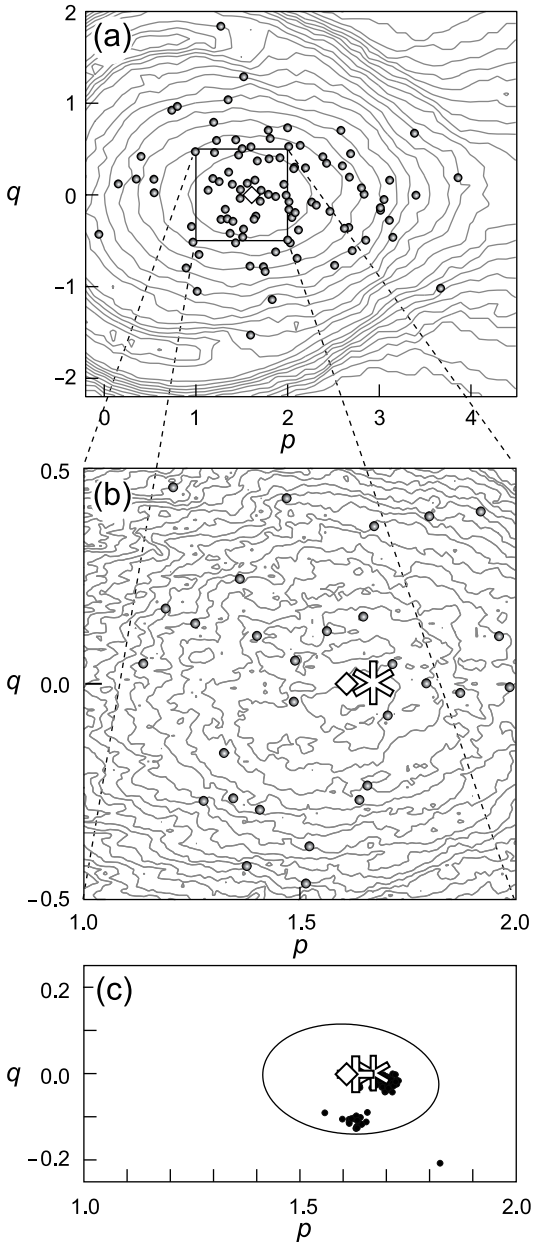

Fig. 11. (a) Elliott plot of artificial data with pre-strain isotropic fabric. Gray contours show the χ^2 statistic, the object function of the θ-curve method (Lisle, 1977b) applied to the data. Diamond designates the assumed strain with which the artificial data were generated. (b) Contours showing the χ^2 statistic near the point (bold asterisk) where the function has the minimum. (c) Filled circles indicate the optimal solutions obtained by the jackknife method for the θ-curve method applied to the artificial data. The ellipse centered by a bold cross shows the standard confidence region of the optimal point determined by the present method. Asterisk shows the optimal point for the θ-curve method applied to the whole data.

Note that the contours in Fig. 11 are not smooth, indicating the roughness of the surface $\chi^2(p_{\mathrm{s}},q_{\mathrm{s}})$. There are local minima and maxima around the optimal point (Fig. 11). The roughness makes the search for the optimal point difficult. The optimal point indicated by an asterisk in Fig. 11b was found by the downhill simplex method with the initial point that has the minimum χ^2 statistic among the computational grid points with intervals of 0.01 on the Elliott plot.

The roughness also results in computational instability of the optimal point. The instability was demonstrated by the jackknife method (Efron, 1982). Namely, the jth datum was left out to make $(n-1)$ resampled data, where $n=100$ for this case and $j=1,\ldots,$ or n. The optimal strain was determined by the θ-curve method for each resampled dataset. The resampling simulated sampling bias. The optimal points for the datasets were scattered (Fig. 11c), although only one datum was removed from the original dataset. In contrast, the present method showed no such instability. From the resampled datasets, the present method yielded the optimal solutions, which were plotted almost at the same point in Fig. 11c.

The instability is inevitable for strain inversion that assumes initial uniform orientations but does not incorporate initial aspect ratios in its object function. Suppose that the trial point $\boldsymbol{x}_{\mathrm{s}}$ moves over a data point $\boldsymbol{x}_{\mathrm{f}}$ from point A to D in Fig. 12. The corresponding initial point moves from A′ to D′ near the origin, and the initial orientation ϕ_{i} changes from A″ to D″. Although the movement of $\boldsymbol{x}_{\mathrm{i}}$ is continuous from B′ to C′, the orientation jumps from B″ to C″. This jump gives rise to discontinuous changes in $N_{\mathrm{i}}(\boldsymbol{x}_{\mathrm{s}})$, and results in the roughness of the object function. Since the optimal point exits in the vicinity of the center of mass $\bar{\boldsymbol{x}}_{\mathrm{f}}$ (Lisle, 1977a), the roughness of the surface makes local minima around the optimal point.

Moriyama and Wallis (2002) attempted to evaluate the

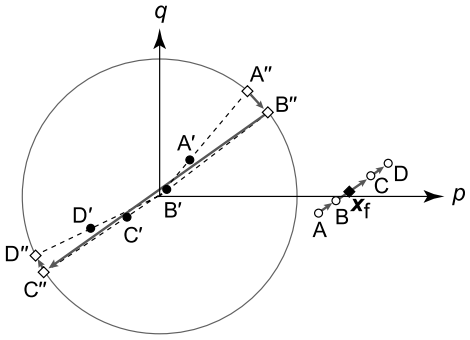

Fig. 12. Schematic picture showing origin of the instability of the θ-curve method. Solid diamond indicates the data point $\boldsymbol{x}_{\mathrm{f}}$. Open circles A–D depict trial points for $\boldsymbol{x}_{\mathrm{s}}$. The back projection of $\boldsymbol{x}_{\mathrm{f}}$ with the trial points results in the initial points depicted by solid circles A′–D′, the tangential coordinates of which are indicated by diamonds A″–D″ on the unit circle. The coordinate jumps from B″ to C″ during the passage of $\boldsymbol{x}_{\mathrm{s}}$ near $\boldsymbol{x}_{\mathrm{f}}$.

confidence region of the optimal strain in the range where χ^2 was smaller than a threshold. However, this is not necessarily a simply connected region due to the roughness, even if the uniform distribution of initial orientations is valid. Consequently, error estimation is not straightforward for the conventional R_f/ϕ technique that assumes only a uniform initial orientation. The instability is removed by taking not only those orientations but also initial aspect ratios in object function. For this reason, the inverse method proposed in this article has the smooth object function $T^2(\boldsymbol{x}_s)$, and can determine an optimal strain without such instability, even if the mean $\bar{x}_i$ of initial fabric was displaced from the origin (Section 8.2).

10. Discussion

It is obvious that the limitation of the present method comes from the assumption that pre-strain fabric is characterized by a bivariate normal distribution with the mean at the origin of the Elliott plot. Although this specific distribution is expected, the present method can evaluate strain and its error from R_f/ϕ data that were not suitable for existing methods.

Unfortunately, we have not got enough examples to test the validity of the assumption for sedimentary grains, because there are only a small number of sedimentological studies describing the relationship between the shape and orientation of grains (e.g. Lindsay, 1968; Seymour and Boulter, 1979; Paterson and Yu, 1994). Recently, Yamaji and Masuda (2005) pointed out the significance of this relationship in the sedimentological community.

The bivariate normal distribution is expected as an approximation, as exemplified by the natural data with a weak initial anisotropy in Figs. 2 and 7. Grains that literally have such a distribution are characterized by the bimodal major-axis orientations with intervals of $\sim 90°$. Sedimentary particles have this tendency upon bedding planes (Potter and Pettijohn. 1963, p. 44). Undeformed clastic grains have $1/R_i$ obeying normal distributions (Griffiths, 1967). It should be noted that this is compatible with our bivariate normality. The former concerns a one-dimensional frequency distribution, and the latter is a two-dimensional distribution. Table 3 shows that the grains in Fig. 2 have basic statistics consistent with the normal distribution of $1/R_i$ given by Griffiths (1967). Yet, extensive studies on the relationship of aspect ratios and orientations is obviously needed to improve strain analysis.

The bivariate normality is the simplest assumption for two-dimensional parametric distribution of points. There is no way to evaluate strain from R_f/ϕ data without assuming some initial fabric. It was demonstrated in Section 9 that our assumption is better than uniform initial orientations. The latter has been the most popular assumption, but such a random fabric is unlikely for actual sedimentary grains (Griffiths, 1967). It was, therefore, recommended to test this assumption using the symmetric or asymmetric distribution of data points on the R_f/ϕ diagram before determining the optimal strain ellipse (Lisle, 1985). If the distribution has an asymmetric tail like that in Fig. 5d, the points making up the tail are left out of analysis to cope with the initial anisotropy.

A few previous researchers (e.g. Elliott, 1970) have taken not only pre-strain orientations but also aspect ratios. Among them, Wheeler (1984) assumed a pre-strain fabric similar to an isotropic bivariate normal distribution just like the case of Fig. 5a. A recent method by Mulchrone et al. (2003) assumes the uniform orientations and pre-strain axial ratios independent of the orientations. Consequently, the distribution of initial points that they expect has a rotational symmetry about the origin of the Elliott plot, including the case of Fig. 5a and an annular peak around the origin. If the initial fabric has a pattern similar to Fig. 5a, these two methods and the present one will determine largely the same optimal strains. Mulchrone et al. (2003) attempted to extend the strain inversion of R_f/ϕ data to the cases of arbitrary distribution of initial aspect ratios. In contrast, the present method takes anisotropic initial fabric into account.

The present method can stably determine the optimal strain. In addition, the present assumption allows us to evaluate the confidence region of the optimal strain, though the evaluation becomes unstable for grains with a small a_1/a_4 ratio that indicates a strong initial fabric. However, the determination of the optimal strain is numerically stable for such a dataset. If grains have such an initial anisotropy, R_f/ϕ data are not enough for strain analysis (De Paor, 1980).

Acknowledgements

The author is grateful to R.J. Lisle, K.F. Mulchrone and B. Owen for constructive comments to early versions of the manuscript. Thanks are also due to T. Shimamoto and

Table 3
Basic statistics of $1/R_i$ for clastic grains

	Mean	Standard deviation	Skewness	Kurtosis
Average (min/max)	0.685 (0.629/0.729)	0.150 (0.138/0.173)	0.099 (−0.345/0.120)	2.68 (2.01/3.01)
Fig. 2a	0.645	0.152	−0.184	2.54
Fig. 2b	0.678	0.139	−0.307	2.57

Values in the upper two rows are after Griffiths (1967, p. 123) who tabulates the statistics for quartz grains in sands and sandstones in various areas. Mean, standard deviation, skewness and kurtosis for the quartz grains are listed in the row with the label 'Average', and the paired figures in parentheses indicate the range of each statistic. Values listed in the lower two rows show the values for the grains of which Elliott plots are illustrated in Fig. 2.

F. Masuda for discussion and for the use of thin sections, respectively. Financially supported by JSPS (No. 14540423).

References

Borradaile, G.J., 1976. A study of a granite/granite-gneiss transition and accompanying schistosity formation in SE Spain. Journal of the Geological Society, London 132, 417–428.

Cloos, E., 1947. Oolite deformation in the South Mountain Fold, Maryland. Bulletin of Geological Society of America 58, 843–918.

De Paor, D.G., 1980. Some limitations of the R_f/ϕ technique of strain analysis. Tectonophysics 64, T29–T31.

De Pree, C.G., Axelrod, A. (Eds.), 2003. Van Nostrand's Concise Encyclopedia of Science and Technology. Wiley, Orlando.

Dunnet, D., 1969. A technique of finite strain analysis using elliptical particles. Tectonophysics 7, 117–136.

Dunnet, D., Siddans, A.W.B., 1971. Non-random sedimentary fabrics and their modification by strain. Tectonophysics 12, 307–325.

Efron, B., 1982. The Jackknife, the Bootstrap, and Other Resampling Plans. Society for Industrial and Applied Mathematics, Philadelphia.

Elliott, D., 1970. Determination of finite strain and initial shape from deformed elliptical objects. Geological Society of America Bulletin 81, 222–2236.

Griffiths, J.C., 1967. Scientific Method in Analysis of Sediments. McGraw-Hill, New York.

Hayashi, D., 1999. Factors controlling precision of 3D strain analysis using ellipsoidal passive markers. Geoinformatics 10, 129–142.

Johnson, R.A., Wichern, D.W., 2002. Applied Multivariate Statistical Analysis, 5th ed. Prentice-Hall, Upper Saddle River, NJ.

Kanatani, K., 1996. Statistical Optimization for Geometric Computation: Theory and Practice. Elsevier, Amsterdam.

Lindsay, J.F., 1968. The development of clast fabric in mudflows. Journal of Sedimentary Petrology 38, 1242–1253.

Lisle, R.J., 1977a. Estimation of the tectonic strain ratio from the mean shape of deformed elliptical markers. Geologie en Mijnbouw 56, 140–144.

Lisle, R.J., 1977b. Clastic grain shape and orientation in relation to cleavage from the Aberystwyth Grits, Wales. Tectonophysics 39, 381–395.

Lisle, R.J., 1985. Geological Strain Analysis: A Manual for the R_f/ϕ Method. Pergamon Press, Oxford.

Masuda, F., Suzaki, K., 1984. Oriented thin section of unconsolidated sands and its sedimentological significance. Report of the Center of Hydraulics, Tsukuba University 8, 17–28 (in Japanese).

Matthews, P.E., Bond, R.A.B., Van Den Berg, J.J., 1974. An algebraic method of strain analysis using elliptical markers. Tectonophysics 24, 31–67.

Moriyama, Y., Wallis, S., 2002. Three-dimensional finite strain analysis in the high-grade part of the Sanbagawa Belt using deformed meta-conglomerate. The Island Arc 11, 111–121.

Moss, A.J., 1963. The physical nature of common sandy and pebbly deposits. American Journal of Science 261, 182–193.

Moss, A.J., 1966. Origin, shaping and significance of quartz sand grains. Journal of Geological Society of Australia 13, 97–136.

Mulchrone, K.F., Meere, P.A., 2001. A Windows program for the analysis of tectonic strain using deformed elliptical markers. Computers and Geosciences 27, 1253–1257.

Mulchrone, K.F., O'Sullivan, F., Meer, P.A., 2003. Finite strain estimation using the mean radial length of elliptical objects with bootstrap confidence intervals. Journal of Structural Geology 25, 529–539.

Paterson, S.R., Yu, H., 1994. Primary fabric ellipsoids in sandstones: implications for depositional process and strain analysis. Journal of Structural Geology 16, 505–517.

Potter, P.E., Pettijohn, F.J., 1963. Paleocurents and Basin Analysis. Springer, Berlin.

Press, W.H., Teukolsky, S.A., Vetterling, W.T., Flannery, B.P., 1993. Numerical Recipes in C: The Art of Scientific Computing, 2nd ed. Cambridge University Press, Cambridge.

Ramsay, J.G., 1967. Folding and Fracturing of Rocks. McGraw-Hill, New York.

Ramsay, J.G., Huber, M.L., 1983. The Techniques of Modern Structural Geology. Volume 1: Strain Analysis. Academic Press, London.

Ribeiro, A., Possolo, A., 1978. Determination of finite strain in deformed planar fabrics. Communicações dos Serviços Geológicos de Portugal 63, 77–81.

Schultz-Ela, D.D., 1990. A method for estimating errors in calculated strains. Journal of Structural Geology 12, 939–943.

Seymour, D.B., Boulter, C.A., 1979. Tests of computerised strain analysis methods by the analysis of simulated deformation of natural unstrained sedimentary fabrics. Tectonophysics 58, 221–235.

Shimamoto, T., Ikeda, Y., 1976. A simple algebraic method for strain estimation from deformed ellipsoidal objects. 1. Basic theory. Tectonophysics 36, 315–337.

Siddans, A.W.B., 1980. Analysis of three-dimensional, homogeneous, finite strain using ellipsoidal objects. Tectonophysics 64, 1–16.

Wheeler, J., 1984. A new plot to display the strain of elliptical markers. Journal of Structural Geology 6, 417–423.

Wheeler, J., 1986. Strain analysis in rocks with pretectonic fabrics. Journal of Structural Geology 8, 887–896.

Yamaji, A., Masuda, F., 2005. Improvements in graphical representation of fabric data, showing the influence of aspect ratios of grains on their orientations. Journal of Sedimentary Research 75, 517–522.

Yu, H., Zheng, Y., 1984. A statistical analysis applied to the R_f/ϕ method. Tectonophysics 110, 151–155.